PLATELETS AND THROMBOPOIESIS

Essential role of class II PI3K-C2α in platelet membrane morphology

Colin Valet,[1] Gaëtan Chicanne,[1] Childerick Severac,[2,3] Claire Chaussade,[4] Maria A. Whitehead,[4] Cendrine Cabou,[1] Marie-Pierre Gratacap,[1] Frederique Gaits-Iacovoni,[1] Bart Vanhaesebroeck,[4] Bernard Payrastre,[1,5] and Sonia Severin[1]

[1]Inserm, U1048-Université Toulouse III, Institut des Maladies Métaboliques et Cardiovasculaires, Toulouse, France; [2]CNRS, ITAV-USR3505, Toulouse, France; [3]Université de Toulouse, ITAV-USR3505, Toulouse, France, [4]UCL Cancer Institute, Paul O'Gorman Building, University College London, London, United Kingdom; [5]Centre Hospitalier Universitaire de Toulouse, Laboratoire d'Hématologie, Toulouse, France

Key Points

- PI3K-C2α controls platelet membrane structure and remodeling.
- PI3K-C2α is a key regulator of a basal housekeeping PI3P pool in platelets.

The physiologic roles of the class II phosphoinositide 3-kinases (PI3Ks) and their contributions to phosphatidylinositol 3-monophosphate (PI3P) and PI(3,4)P_2 production remain elusive. Here we report that mice heterozygous for a constitutively kinase-dead PI3K-C2α display aberrant platelet morphology with an elevated number of barbell-shaped proplatelets, a recently discovered intermediate stage in the final process of platelet production. Platelets with heterozygous PI3K-C2α inactivation have critical defects in α-granules and membrane structure that are associated with modifications in megakaryocytes. These platelets are more rigid and unable to form filopodia after stimulation. Heterozygous PI3K-C2α inactivation in platelets led to a significant reduction in the basal pool of PI3P and a mislocalization of several membrane skeleton proteins known to control the interactions between the plasma membrane and cytoskeleton. These alterations had repercussions on the performance of platelet responses with delay in the time of arterial occlusion in an in vivo model of thrombosis and defect in thrombus formation in an ex vivo blood flow system. These data uncover a key role for PI3K-C2α activity in the generation of a basal housekeeping PI3P pool and in the control of membrane remodeling, critical for megakaryocytopoiesis and normal platelet production and function. (*Blood.* 2015;126(9):1128-1137)

Introduction

Phosphoinositide 3-kinases (PI3Ks) are lipid kinases that produce D3-phosphorylated phosphoinositides, which are able to interact with proteins to organize functional complexes regulating various biological processes including signal transduction, cytoskeletal organization, and vesicular trafficking.[1,2] After stimulation, class I PI3Ks produce phosphatidylinositol 3,4,5 trisphosphate [PI(3,4,5)P_3], a short-lived second messenger involved in signal transduction. In contrast, class II and III PI3Ks are thought to generate phosphatidylinositol 3-monophosphate (PI3P), a lipid that is present at relatively low amounts in cells and that controls vesicular trafficking. Whether class II and III PI3Ks produce both basal and inducible pools of PI3P remain unclear. In addition to PI3P, class II PI3Ks can also produce phosphatidylinositol 3,4 bisphosphate [PI(3,4)P_2].[3] Class II α PI3K (PI3K-C2α), 1 of the 3 members of the class II PI3K subfamily, has become the focus of recent studies, but its exact physiological role still remains enigmatic.[3-8] In vitro studies have implicated PI3K-C2α in intracellular membrane trafficking, endocytosis, exocytosis, and autophagy.[3-5] Recently, loss of the *Pik3c2a* gene in mouse was shown to cause early embryonic lethality (between embryonic day 10.5 and embryonic day 11.5) as a result of severe defects in angiogenesis and vascular barrier function, together with primary cilium organization.[6-8]

More than 15 years ago, the group of Susan Rittenhouse suggested that a class II PI3K could be implicated in blood platelet activation,[9] but to our knowledge, no work has followed since then. Platelets are small, anucleated blood cells that play a vital role in hemostasis and thrombosis. After vascular injury and exposure of the subendothelial matrix, platelets adhere and form an hemostatic plug to prevent excessive blood loss.[10,11] Platelets are produced by megakaryocytes after a highly regulated process of maturation of hematopoietic stem cells into giant polyploid cells, characterized by intense membrane and cytoskeleton remodeling.[12] Mature megakaryocytes extend long, branched structures designated as proplatelets, which cross the endothelial barrier and, under hemodynamic flow, split into young "reticulated" platelets in the bloodstream. Platelet shaping and sizing resulting from reversible conversion of round-shaped platelets into barbell-shaped proplatelets also occurs in the bloodstream, where they undergo successive rounds of fission via membrane and cytoskeleton remodeling to produce mature platelets.[13-20]

To gain insight into the physiological role of PI3K-C2α in platelet production and function, we used a mouse line heterozygous for a germ-line kinase-inactive knock-in (KI) mutation (D1268A) in the endogenous *Pik3c2a* gene. These mice with a heterozygous inactivation of PI3K-C2α were viable and fertile but showed aberrant platelet formation with critical defect in platelet membrane morphology and dynamics and an enrichment of barbell-shaped proplatelets in the bloodstream. Our data demonstrate that PI3K-C2α regulates an agonist-independent pool of PI3P and is important for organizing the membrane skeleton to allow normal platelet production and functions.

Submitted March 24, 2015; accepted June 15, 2015. Prepublished online as *Blood* First Edition paper, June 24, 2015; DOI 10.1182/blood-2015-03-636670.

B.V., B.P., and S.S. share senior authorship of this study.

The online version of this article contains a data supplement.

There is an Inside *Blood* Commentary on this article in this issue.

The publication costs of this article were defrayed in part by page charge payment. Therefore, and solely to indicate this fact, this article is hereby marked "advertisement" in accordance with 18 USC section 1734.

Methods

Animals

Wild-type (WT) and heterozygous mutant mice with inactive PI3K-C2α (WT/D1268A) were of C57BL/6 genetic background and housed in the Anexplo (Toulouse) vivarium according to institutional guidelines. For all experiments, 8- to 14-week-old mice were used. Ethical approval for animal experiments was obtained from the French Ministry of Research in agreement with European Union guidelines.

Preparation of murine platelets, flow assay on collagen, carotid artery thrombosis, and tail bleeding time are described in detail in the supplemental *Methods*.

In vitro PI 3-kinase assay

Platelets (4×10^8) were lysed at 4°C in 20 mM Tris·HCl (pH 7.7), 150 mM NaCl, 4 mM EDTA, 1 mM Na_3VO_4, 10 μg/mL leupeptin and aprotinin, 1 mM phenylmethylsulfonyl fluoride, and 0.5% Triton X-100. Lysates were centrifuged at 16 000*g*, and the supernatants were incubated for 2 hours with anti-PI3K-C2α antibody and protein A-Sepharose beads. Immunoprecipitate was resuspended in kinase assay buffer (20 mM Tris·HCl at pH 7.4, 100 mM NaCl, 0.5 mM EGTA, 10 mM $MgCl_2$, and 100 μM ATP). Then, 10 μg phosphatidylinositol vesicles and 10 μCi γ-[^{32}P] ATP were added, and after 20 minutes at 37°C, under gentle shaking, reaction was terminated and lipids were extracted using the Bligh and Dyer procedure.

Electron microscopy

Platelets were fixed in 2.5% glutaraldehyde in 0.1 M sodium cacodylate buffer at 4°C overnight. After 2 washes in the same buffer, platelets were allowed to adhere on poly-lysine-coated cover glasses and then dehydrated in a graded ethanol series (scanning electron microscopy) or embedded in resin and sectioned (transmission electron microscopy) according to standard procedures for electron microscopy imaging. Tibia bone marrow was flushed and fixed in 2.5% glutaraldehyde in 0.1 M sodium cacodylate buffer at 4°C overnight, embedded in resin, and sectioned (transmission electron microscopy) according to standard procedures for electron microscopy imaging. Samples were analyzed with HT 7700 Hitachi transmission electron microscope or FEG FEI Quanta 250 scanning electron microscope.

Platelet morphology

Freshly isolated platelets were fixed with formalin (2% final), either immediately to assess baseline morphology or after 24 hours of suspension culture in M199 medium (Gibco, Invitrogen). Fixed platelets were subsequently layered onto poly-L-Lysine-coated microscope slides, using a cytospin centrifuge (Shandon Cytospin; Thermo Fisher Scientific). To determine the number of platelets with extensions and distinct cell bodies, fixed cells were counterstained with an anti-α-tubulin antibody and an AlexaFluor488 secondary antibody. Ten random fields were captured, using Zeiss LSM780 confocal and Zen Zeiss software, from each independent experiment, and platelets with two or more distinct cell bodies on the total platelet count were counted. Round platelet diameter was evaluated by line-scan analysis, using Zen Zeiss software, as previously described.[21]

Lipid analysis

PI3P mass assay and phosphoinositide labeling were performed on washed platelets, as previously described.[22,23] To analyze phospholipid and cholesterol, washed platelets were homogenized in 2 mL of a mixture of methanol:5 mM EGTA (2:1, volume to volume ratio [v/v]) and were extracted according to Bligh and Dyer in a chloroform/methanol/water mixture (2.5:2.5:2.1, v/v/v) in the presence of the internal standard (15 μg stigmasterol, phosphatidylethanolamine, 12:0/12:0; phosphatidylcholine, 13:0/13:0; phosphatidylinositol (PI), 16:0/17:0; and phosphatidylserine, 12:0/12:0). Cholesterol quantification was obtained after gas chromatography analysis. To simultaneously separate phospholipids liquid chromatography-tandem mass spectrometry, the previous extract was analyzed on an ultrahigh-performance liquid chromatography system (Agilent LC1290 Infinity) HYLIC column coupled to Agilent 6460 triple quadrupole MS (Agilent Technologies) equipped with electrospray ionization operating in negative and positive mode.

Flow assay on von Willebrand factor

Murine von Willebrand factor (vWF; 10 μg/mL) was immobilized overnight on a surface precoated for 4 hours with a polyclonal anti-human vWF antibody (31 μg/mL; Dako). Washed platelets were perfused in vWF-coated microcapillaries at a shear rate of 18 dynes/cm^2. Real-time adhesion was observed in 3 microscopic fields at ×40 magnification during a 35-minute period, starting 4 minutes after the onset of perfusion (1 frame every 5 seconds).

Atomic force microscopy

A NanoWizard II atomic force microscope (JPK Instruments) mounted on an inverted optical microscope (Axiovert 200; Carl Zeiss MicroImaging) was used to localize platelets, image them, and measure their membrane mechanical forces (Young Modulus). Silicon Nitride cantilevers (MLCT, Bruker) with nominal spring constant of 0.1 N/m, a pyramidal shaped tip, and a half cone angle $\alpha = 17.5°$.

The thermal tune method[24] was systematically used to measure the cantilevers spring constants, which were all found in the range from 0.14 to 0.16 N/m.

Elasticity measurements. All experiments were conducted in N-2-hydroxyethylpiperazine-N′-2-ethanesulfonic acid liquid media and maintained at 37°C, using a temperature-controlled sample holder (BioCell; JPK Instruments). Washed platelets were placed on a fibrinogen-coated surface and left to adhere for 45 minutes in the presence of thrombin (0.5 IU/mL) before any experiments. Force (F) vs displacement curves were recorded according to a 16×16 matrix over a 1.5×1.5 μm^2 area for each platelet, with a maximum load of 4 nN to preserve membrane integrity. These curves were then converted into indentation (δ) curves and fitted using JPK Instruments data processing software with the conical hertz model[25] of Equation 1 with a Poisson ratio (ν) arbitrary fixed to 0.5:

$$F = \frac{2\,E\,tan\,\alpha}{\pi(1-\nu^2)}\delta^2 \quad (1)$$

For each force curve, the Young's modulus (E) is calculated and plotted on histograms.

Atomic force microscopy imaging. After adhesion, platelets were fixed in 1.5% formalin solution for 30 minutes and then washed and imaged in air at room temperature. The atomic force microscopy (AFM) scanner has a maximum range of 100 μm in XY directions and 15 μm in the vertical direction. Images were acquired at 512 × 512 pixel resolution at a line rate of 1 to 2 Hz with a maximum applied force of 4 nN. All images were analyzed using JPK data processing software. Linear plan fit was used to remove sample tilt from height images, using the glass slide as the zero reference plan.

Isolation of membrane skeleton

Platelets were lysed by the addition of ice-cold cytoskeleton buffer (100 mM Tris·HCl at pH 7.4, 20 mM EGTA, 2 mM Na_3VO_4, 4 μg/mL each of aprotinin and leupeptin, 2 mM phenylmethylsulfonyl fluoride, and 2% Triton X-100) for 10 minutes at 4°C. Platelet membrane skeleton (Triton X-100 insoluble fraction) was isolated from the 16 000*g* supernatant by centrifugation at 100 000*g* overnight and then solubilized and prepared for sodium dodecyl sulfate-polyacrylamide gel electrophoresis.

Statistical analysis

Data are expressed as mean ± standard error of the mean. Significance of differences was determined using 2-tailed Student t test or 2-way analysis of variance or 1-sample t test. P values $< .05$ were considered significant (*$P < .05$, **$P < .01$, ***$P < .001$).

Results

PI3K-C2α$^{WT/D1268A}$ mice display defects in platelet formation and membrane morphology

To investigate the role of PI3K-C2α in platelets, we used a mouse line with a germline kinase-inactivating KI mutation in the PI3K-C2α protein, further referred to as PI3K-C2α^{D1268A}. Whereas homozygous KI mice are embryonic lethal, heterozygous mice (hereafter called PI3K-C2α$^{WT/D1268A}$ mice) are born at the expected Mendelian ratio, are viable and fertile, and develop normally, with no apparent morphological abnormalities (B.V., manuscript in preparation). PI3K-C2α$^{WT/D1268A}$ mice showed no signs of spontaneous bleeding compared with littermate WT mice and had comparable levels of *Pik3c2a* mRNA level in megakaryocytes and unaltered protein expression of PI3K-C2α and other class I, II, and III PI3K isoforms in platelets (Figure 1A-B). PI3K-C2α immunoprecipitates from PI3K-C2α$^{WT/D1268A}$ platelets displayed a 50% reduction in lipid kinase activity (Figure 1B), in line with heterozygous inactivation of PI3K-C2α.

Except for hematocrit, which was slightly enhanced, basic blood parameters such as red/white blood cell count, hemoglobin concentration, and mean globular volume, as well as immune cell populations (B cells, T cells, granulocytes), were unaltered in PI3K-C2α$^{WT/D1268A}$ mice (Table 1). PI3K-C2α$^{WT/D1268A}$ mice displayed a normal platelet count (Figure 1C). However, although the mean volume of platelet population was not significantly different (7.70 $\mu m^3 \pm 0.27$ μm^3 for PI3K-C2α$^{WT/D1268A}$ vs 7.16 $\mu m^3 \pm 0.25$ μm^3 for WT; n = 30 mice), platelets were heterogeneous in size, as reflected by increased platelet distribution width in PI3K-C2α$^{WT/D1268A}$ mice compared with in WT mice (3.76% ± 0.41% vs 2.82% ± 0.22%; n = 30 mice; $P < .05$) and confirmed by tubulin ring diameter measurement (Figure 1C; supplemental Figure 1, available on the *Blood* Web site). Expression levels of major platelet surface receptors were comparable in PI3K-C2α$^{WT/D1268A}$ and WT platelets (Figure 1C). Transmission electron microscopy analysis revealed an abnormal ultrastructure of resting PI3K-C2α$^{WT/D1268A}$ platelets, with major defects in membrane morphology including an aberrant invaginated and tortuous shape of the plasma membrane as compared with the smooth plasma membrane from WT platelets (Figure 1D). The open canalicular system, which represents invaginations of the plasma membrane and constitutes a reservoir of membranes necessary for platelet shape change during activation, appeared altered in PI3K-C2α$^{WT/D1268A}$ platelets (Figure 1D). Quantification indicated that 31% ± 5.4% of PI3K-C2α$^{WT/D1268A}$ platelets have an invaginated and rough morphology compared with 4.2% ± 2.2% of WT platelets. The winding plasma membrane shape of PI3K-C2α$^{WT/D1268A}$ platelets was confirmed by scanning electron microscopy (Figure 1D). Strikingly, an enrichment of platelets with 2 cell bodies, recently named barbell-shaped proplatelets,[19] which are normally very rare, was observed in PI3K-C2α$^{WT/D1268A}$ platelet suspension (Figure 1D). In addition, PI3K-C2α$^{WT/D1268A}$ platelets displayed an abnormal α-granule distribution characterized by 46.0% ± 1.2% reduction in number and 60.5% ± 3.7% increase in size compared with WT platelets (Figure 1E). Global platelet α-granule content such as vWF and fibrinogen was, however, not altered. Transmission electron microscopy, mepacrine uptake, and serotonin quantification showed no substantial difference in the number, size, and content of dense granules between WT and PI3K-C2α$^{WT/D1268A}$ platelets (supplemental Figure 2). Despite membrane and α-granule defects, but consistent with a normal platelet count, the in vivo life span of PI3K-C2α$^{WT/D1268A}$ platelets and their count recovery after immune-induced thrombocytopenia was similar to that of WT platelets (supplemental Figure 3).

The defects in membrane and α-granules were already observed in PI3K-C2α$^{WT/D1268A}$ megakaryocytes, as shown by transmission electron microscopy analysis of the native bone marrow. The demarcation membrane system was less developed and delineated compared with WT megakaryocytes (Figure 1F). Fewer α-granules, heterogeneous in shape and bigger than in WT, were also observed in PI3K-C2α$^{WT/D1268A}$ megakaryocytes (Figure 1F).

Altogether, these data point to a critical role for PI3K-C2α in the organization of membrane structure and platelet morphology, already detectable in megakaryocytes.

PI3K-C2α$^{WT/D1268A}$ platelets have a reduction in the basal, agonist-insensitive, pool of PI3P

Whether class II PI3Ks control a basal or a stimulation-sensitive pool of PI3P, or both, remains unclear. Emerging evidence suggests class II PI3Ks can also generate PI(3,4)P_2 under certain conditions.[3] We used 3 complementary methods to analyze phosphoinositide levels in PI3K-C2α$^{WT/D1268A}$ platelets: high-performance liquid chromatography analysis after short-term (45 minutes) ^{32}P-labeling of platelets, efficient in determining the fast turnover of phosphoinositides and their acute changing after stimulation[26]; a PI3P-specific mass assay to measure the total amount of PI3P[22]; and imaging using the PI3P-binding FYVE^{HRS} domain as a probe. High-performance liquid chromatography analysis of the short-lived phosphoinositide pools did not show any significant differences in the basal or agonist-stimulated levels of PI3P or other phosphoinositides, including PI(3,4)P_2 and PI(3,4,5)P_3 (Figure 2A; supplemental Figure 4). However, as PI3P also exists in a pool with slow turnover time, we next used a PI3P-specific mass assay and found a 29.7% ± 3.3% decrease in PI3P in resting PI3K-C2α$^{WT/D1268A}$ platelets compared with WT (Figure 2B). This decrease was highly significant, given that only 50% of the PI3K-C2α was inactivated, suggesting PI3K-C2α contributes to about half of the basal PI3P level in WT platelets. The decrease in basal PI3P pool in resting PI3K-C2α$^{WT/D1268A}$ platelets was confirmed by immunofluorescence staining with the FYVE^{HRS} probe (40.3% ± 3.3% decrease in PI3K-C2α$^{WT/D1268A}$ platelets compared with WT platelets; Figure 2C). In platelets stimulated with collagen-related peptide (CRP) or thrombin, the amount of PI3P was found to increase and reach comparable levels in WT and PI3K-C2α$^{WT/D1268A}$ platelets (Figure 2A-B). Overall, these data show that PI3K-C2α does not significantly contribute to the agonist-inducible pool of PI3P in platelets, but interestingly, it produces a major fraction (~50%) of the basal, housekeeping, pool of PI3P. This pool of PI3P likely has a slow turnover, as short-term (45 minutes) ^{32}P-labeling did not reveal significant differences between WT and PI3K-C2α$^{WT/D1268A}$ platelets.

PI3K-C2α$^{WT/D1268A}$ mice display an enrichment of barbell proplatelets in the bloodstream and a decrease in platelet filopodia formation

To further investigate the enrichment of barbell-shaped proplatelets observed in PI3K-C2α$^{WT/D1268A}$ mice by transmission electron microscopy (Figure 1D), we analyzed freshly obtained washed platelets or washed platelets cultured in suspension for 24 hours, which is known to increase the level of barbell-shaped proplatelets.[17] The percentage of platelets with 2 cell bodies was dramatically increased in PI3K-C2α$^{WT/D1268A}$ samples compared with in WT samples (Figure 3A). A similar increase was observed after perfusion

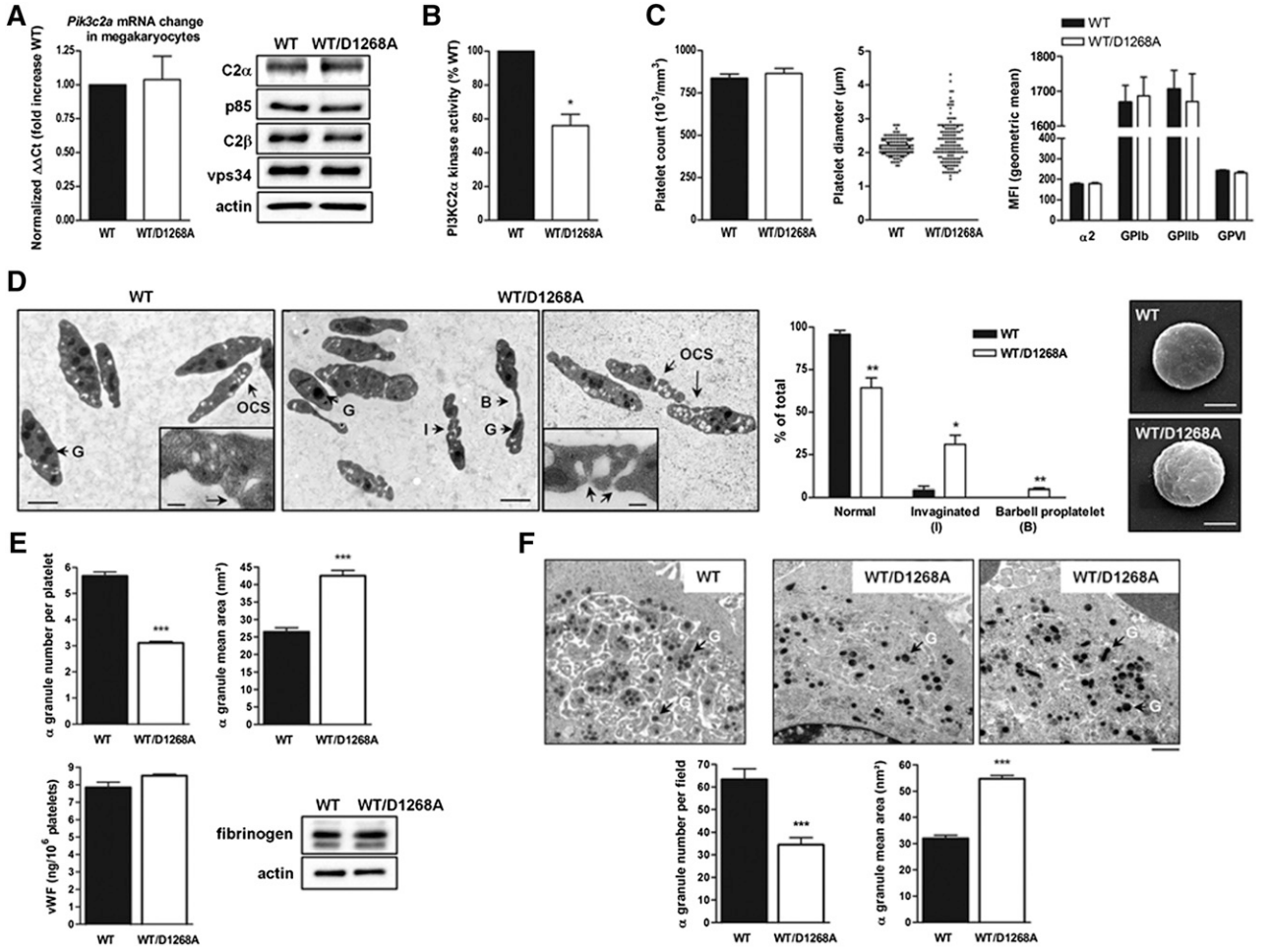

Figure 1. PI3K-C2α regulates platelet biogenesis. (A) Megakaryocyte relative *Pik3c2a* mRNA expression normalized to β-actin cDNA (mean ± standard error of the mean [SEM]; n = 4). Western blot analysis for PI3K-C2α, p85, PI3K-C2β, and vps34 in platelet lysates. (B) In vitro platelet PI3K-C2α lipid kinase activity (mean ± SEM; n = 4; $*P < .05$ vs WT according to 1 sample *t* test). (C) Whole-blood platelet count (mean ± SEM; n = 30 mice), measured using Micros60 (Horiba ABX Diagnostics). Platelet diameter measured using line-scan analysis after α-tubulin staining on fixed resting platelets (mean ± SEM; n = 150 platelets). Surface glycoprotein expression on resting platelets (MFI, mean fluorescence intensity; mean ± SEM; n = 4). (D) Transmission and scanning electron microscopy on resting platelets. Images are representative of 5 mice of each genotype. Scale bar: 1 μm. Enlarged pictures of OCS from WT and PI3K-C2α$^{WT/D1268A}$ platelets are shown. Scale bar: 200 nm. I, invaginated platelet; B, barbell shaped-proplatelets; G, α-granule; OCS, open canalicular system. Quantification on transmission electron microscopy images of normal platelets, aberrant platelets (A), and barbell shaped-proplatelets (B) (mean ± SEM; n > 400 platelets; $*P < .05$ and $**P < .01$ vs WT, according to 2-tailed Student *t* test. (E) α-granule number and mean area quantified on transmission electron microscopy images using ImageJ software (mean ± SEM; n = 100 platelets; $***P < .001$ vs WT, according to 2-tailed Student *t* test). Quantification of vWF by enzyme-linked immunosorbent assay test and fibrinogen by western blotting on resting platelets (mean ± SEM; n = 3). (F) Transmission electron microscopy of mice bone marrow section (n = 3). Scale bar: 2 μm. G; α-granule. α-granule number and mean area quantified as (E) (mean ± SEM, n = 20 megakaryocytes, $***P < .001$ vs WT, according to 2-tailed Student *t* test).

of platelets over a vWF-coated microcapillary for 30 minutes at 18 dynes/cm^2, which is another mean to increase the percentage of barbell-shaped proplatelets[16] (Figure 3B; supplemental Videos 1 and 2). These data reveal a significant increase in the amount of platelets with 2 cell bodies upon heterozygous inactivation of PI3K-C2α, suggesting a defect in the scission required to produce mature platelets, possibly related to the abnormal membrane structure observed in PI3K-C2α$^{WT/D1268A}$ megakaryocytes and platelets. To make sure the observed phenotype was not a result of defects of the vascular endothelium during delivery of platelets into vessel sinusoids, we performed bone marrow transplantation experiments. As shown in Figure 3C, a similar accumulation of platelets with 2 cell bodies was observed when hematopoietic cells carrying the PI3K-C2α$^{WT/D1268A}$ mutation were grafted into a WT or a PI3K-C2α$^{WT/D1268A}$ recipient, and conversely. Thus, the enrichment in barbell-shaped proplatelets observed in PI3K-C2α$^{WT/D1268A}$ mice is a result of a defect of hematopoietic cells.

To further analyze the membrane abnormalities of PI3K-C2α$^{WT/D1268A}$ platelets, we investigated the platelet shape change mechanism by scanning electron microscopy. Although PI3K-C2α$^{WT/D1268A}$ platelets were able to exhibit shape change after

Table 1. Blood parameters

	WT (n = 28)	WT/D1628A (n = 31)
WBC, 10^3/mm^3	3.8 ± 0.3	4.4 ± 0.4
RBC, 10^6 /mm^3	7.2 ± 0.2	7.6 ± 0.2
HGB, g/dL	9.1 ± 0.3	9.6 ± 0.2
HCT, %	31.8 ± 0.9	34.2 ± 0.5*
MGV, μm^3	47 ± 0.2	47.8 ± 0.3

Whole-blood parameters were analyzed with an automated blood analyzer Micros60 (Horiba ABX diagnostics). Mean ± SEM; $*P < .05$ vs WT according to 2-tailed Student *t* test.

HCT, hematocrit; HGB, hemoglobin; MGV, mean globular volume; RBC, red blood cells; WBC, white blood cells.

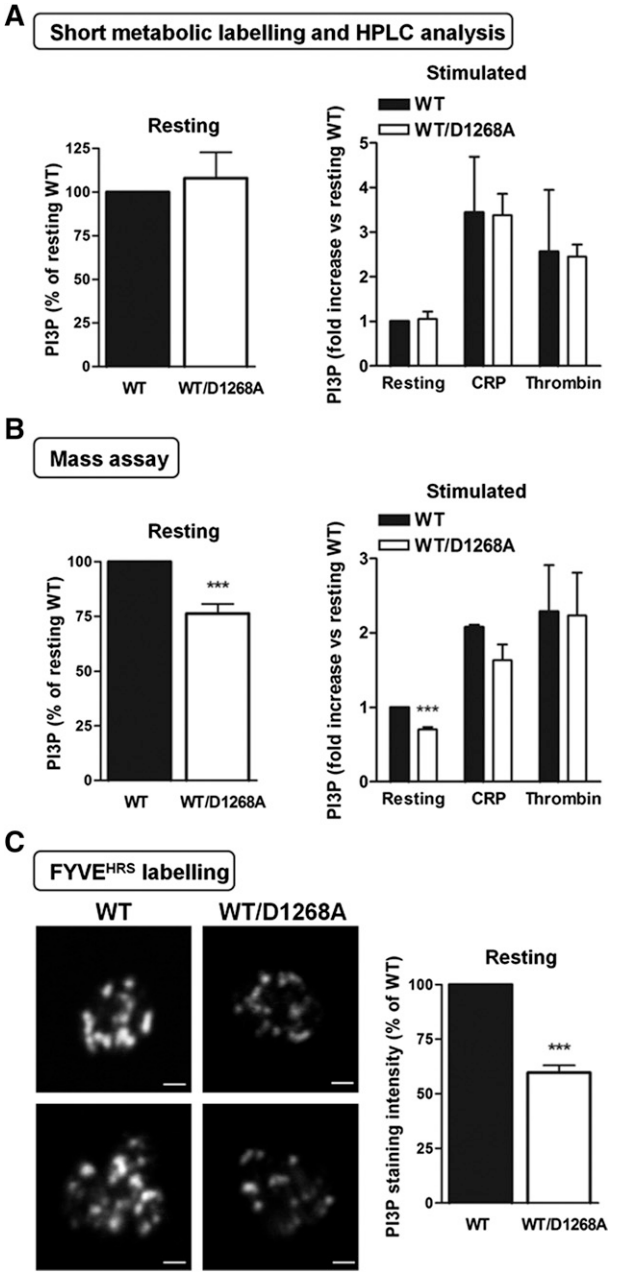

Figure 2. PI3K-C2α is critical for the regulation of basal PI3P level in platelets. (A) High-performance liquid chromatography analysis of PI3P levels in resting and stimulated (10 μg/mL CRP and 0.5 IU/mL thrombin for 3 minutes) ^{32}P-labeled platelets (mean ± SEM; n = 4). (B) PI3P mass assay in resting and stimulated (10 μg/mL CRP and 0.5 IU/mL thrombin for 3 minutes) platelets. The assay was performed as previously described.[22] Briefly, platelet phosphatidylinositol monophosphate (PIP) fraction purified by lipid extraction and thin-layer chromatography was submitted to specific phosphorylation by recombinant PIKfyve, in the presence of [γ-^{32}P]ATP. PIKfyve only phosphorylates PI3P to produce [^{32}P]-PI(3,5)P_2, which reflects the amount of PI3P present in the sample. (mean ± SEM; n = 4; ***$P < .001$ vs WT, according to 1 sample *t* test). (C) Resting platelets were fixed and stained with simple FYVE^{HRS} probe coupled to 647-AlexaFluor. Representative confocal images of FYVE^{HRS}-647 AlexaFluor labeled platelets are shown. Scale bar: 1 μm. Staining intensity in platelets were quantified by ImageJ software (mean ± SEM; n = 3; ***$P < .001$ vs WT, according to 1-sample *t* test).

stimulation by CRP or thrombin in suspension, they showed a dramatic defect in filopodia extension (Figure 4A). The decrease in scission highlighted by the elevated percentage of barbell-shaped proplatelets, the defect in filopodia extension, and the winding plasma membrane shape of resting PI3K-C2α$^{WT/D1268A}$ platelets suggested a reduction in platelet elasticity. Therefore, we used AFM operating in force distance mode to measure platelet compliance by quantifying the Young's modulus. WT and PI3K-C2α$^{WT/D1268A}$ platelets were stimulated by thrombin and allowed to adhere and to spread on fibrinogen to similar extent (supplemental Figure 5). AFM height images revealed numerous membrane invaginations (Figure 4B, see arrows), leading to a tortuous and rough aspect of PI3K-C2α$^{WT/D1268A}$ platelets compared with the homogeneous smooth WT platelet surface (Figure 4B). In line with the electron microscopy analysis, these data indicated an inhomogeneity in PI3K-C2α$^{WT/D1268A}$ platelet membrane. Interestingly, PI3K-C2α$^{WT/D1268A}$ platelets displayed a significantly higher Young's modulus (40.7 kPa ± 3.7 kPa for WT platelets and 62.2 kPa ± 5.4 kPa for PI3K-C2α$^{WT/D1268A}$ platelets) showing an increased rigidity of the latter (Figure 4B). Altogether, these results demonstrate an important role of PI3K-C2α in the control of membrane morphology and biophysical properties.

PI3K-C2α$^{WT/D1268A}$ platelets have normal major lipid composition but aberrant membrane skeleton with repercussion for thrombosis

To gain insight into the mechanisms leading to the observed platelet phenotype, we analyzed potential modifications in the membrane major lipid composition and the spectrin-based membrane skeleton that can affect both membrane structure and dynamics. We first performed a targeted mass-spectrometry-based lipidomic analysis of WT and PI3K-C2α$^{WT/D1268A}$ platelets. No difference in cholesterol, phospholipid, and fatty acid content was observed (Figure 5A), indicating that heterozygous inactivation of PI3K-C2α had no effect on the composition of major membrane lipids. The spectrin-based membrane skeleton is critical for biophysical membrane properties, both in platelets and megakaryocytes,[27,28] and is essential for the conversion from preplatelets to barbell-shaped proplatelets and to mature platelets.[15,19] The membrane skeleton of WT and PI3K-C2α$^{WT/D1268A}$ platelets was isolated, and its composition analyzed by immunoblotting. Although the level of cortical polymerized actin was normal, a significant decrease of cortical spectrin and myosin was observed in PI3K-C2α$^{WT/D1268A}$ platelets compared with in WT platelets (Figure 5B). The presence of proteins known to link plasma membrane to the cytoskeleton such as moesin, filamin, GPIbα, and GPIIb was also decreased in the membrane skeleton of PI3K-C2α$^{WT/D1268A}$ platelets, whereas vinculin levels were not affected (Figure 5B). These differences were not a result of a decrease in the whole-cell lysates expression level of these proteins (Figure 5B; supplemental Figure 6), nor a decrease in the surface expression of GPIb and GPIIb (Figure 1C). Therefore, PI3K-C2α activity appears to be critical for the recruitment and/or stabilization of several membrane skeleton proteins that are required for normal membrane shape and dynamics in platelets.

We next tested whether the morphological defects observed in PI3K-C2α$^{WT/D1268A}$ platelets affected platelet functions in vitro, ex vivo, and in vivo. The in vitro platelet aggregation in response to thrombin, thromboxane A2 analog, or adenosine diphosphate was normal. A decreased aggregation response to low doses of collagen or CRP was observed, but increasing the doses of agonists restored a normal response (supplemental Figure 7). Analysis of acute signaling through Akt or myosin light chain phosphorylation did not point to a role for PI3K-C2α in these events, even in response to low doses of GPVI agonists (supplemental Figure 7), suggesting the platelet aggregation defect was related to changes in membrane structure, rather than signaling defect. In vivo, no significant effect on tail bleeding was observed of PI3K-C2α$^{WT/D1268A}$ mice, suggesting primary hemostasis was spared (Figure 6A). To investigate the potential effect of the

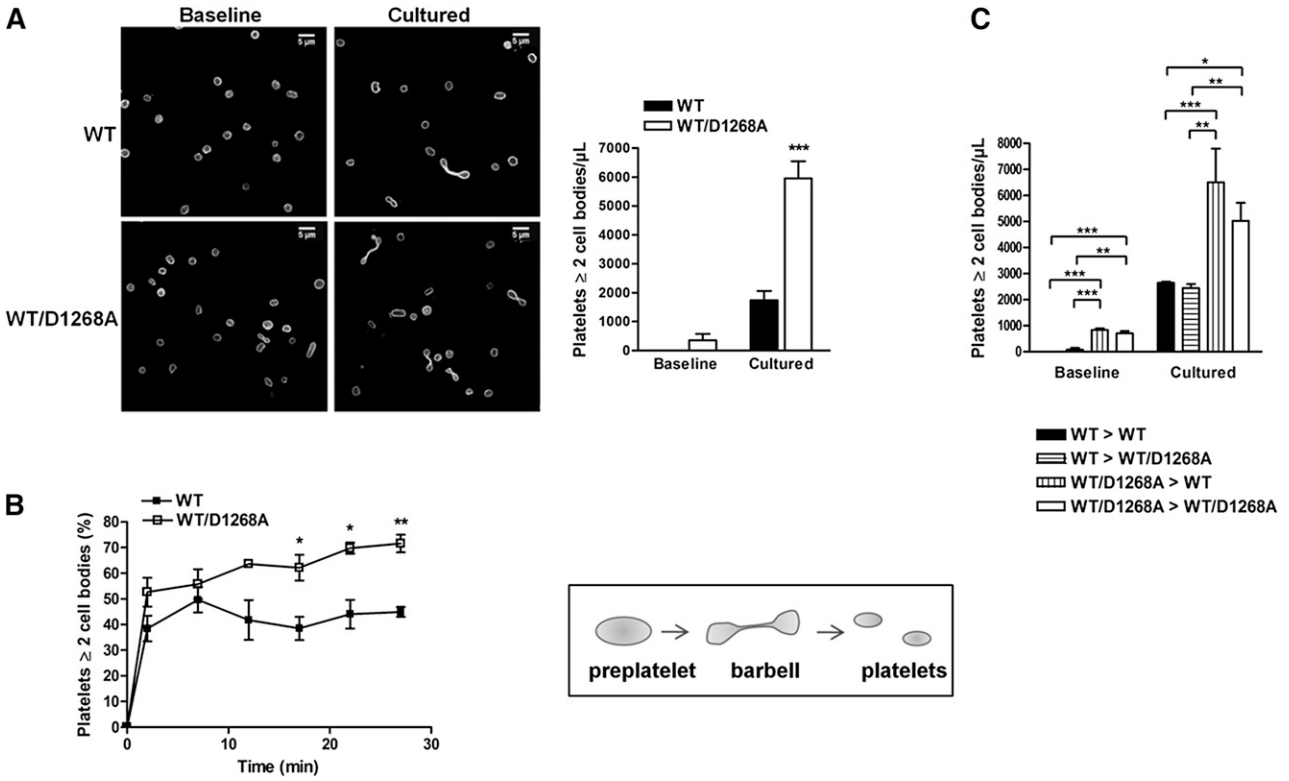

Figure 3. Barbell-shaped proplatelet enrichment in PI3K-C2α$^{WT/D1268A}$ mice. (A) Washed platelets were immediately fixed (baseline) or cultured in suspension for 24 hours (cultured). Panels display a representative example where the platelets were stained for α-tubulin. Scale bar: 5 μm. The bar graph indicates the number of platelets with at least 2 cell bodies per microliter (mean ± SEM; n = 4; ***$P < .001$ vs WT according to 2-tailed Student *t* test). (B) Washed platelets were perfused on murine vWF-coated microcapillaries at 18 dynes/cm^2. 2 cell bodies platelets and discoid platelets were visualized by real-time videomicroscopy. The percentage of 2 cell bodies platelets on total platelets was calculated (mean ± SEM; n = 3; *$P < .05$ and **$P < .01$ vs WT according to 2-tailed Student *t* test). Schematic representation of dynamic platelet release from preplatelets through barbell-shaped proplatelets. (C) Washed platelets from WT mice transplanted with WT bone marrow (WT > WT), PI3K-C2α$^{WT/D1268A}$ mice transplanted with WT bone marrow (WT > WT/D1268A), WT mice transplanted with PI3K-C2α$^{WT/D1268A}$ bone marrow (WT/D1268A > WT), and PI3K-C2α$^{WT/D1268A}$ mice transplanted with PI3K-C2α$^{WT/D1268A}$ bone marrow (WT/D1268A > WT/D1268A) mice were treated as described in A (mean ± SEM; n = 3; *$P < .05$, **$P < .01$, and ***$P < .001$, according to 2-way ANOVA).

PI3K-C2α inactivation on the prothrombotic function of platelets, we analyzed arterial thrombus formation after injury of the mouse carotid with ferric chloride. A significant delay in artery occlusion was observed in PI3K-C2α$^{WT/D1268A}$ mice compared with WT mice (Figure 6B). Ex vivo thrombus formation assay performed on a collagen matrix at arterial shear rate also showed a significant reduction in the prothrombotic capacity of PI3K-C2α$^{WT/D1268A}$ platelets (Figure 6C). These data indicate that the membrane defects arising from PI3K-C2α inactivation have little effect on platelet aggregation in vitro but affect the prothrombotic platelet function observed under arterial shear stress.

Discussion

Using a mouse model of partial inactivation of PI3K-C2α, we show that the kinase activity of this class II isoform of PI3K is essential for normal platelet formation. The most striking phenotype is a defect in membrane morphology and dynamics in platelets and megakaryocytes. PI3K-C2α$^{WT/D1268A}$ platelets are heterogeneous in size with a winding and wrinkled aspect plasma membrane, altered open canalicular system, and defects in α-granules. We show, for the first time, a role for a lipid kinase in the mechanism of terminal platelet production in the bloodstream, with an effect on the generation of barbell-shaped proplatelets. Megakaryocytes release into the sinusoid blood vessels large preplatelet intermediates that convert into barbell-shaped proplatelets and further fragment into platelets in the circulation.[13,17,29,30] Barbell-shaped proplatelet conversion, as well as platelet shape and size, are determined by the balance of microtubule bundling, elastic bending forces linked to membrane biophysical properties, and compressive pressure of the membrane skeleton.[19] In agreement with the profound defect on membrane morphology, PI3K-C2α$^{WT/D1268A}$ platelets are more rigid than normal platelets, as determined by atomic force microscopy. As a consequence, partial inactivation of PI3K-C2α decreases the performance of barbell-shaped proplatelets when undergoing scission, which leads to an accumulation of 2 cell bodies' platelets in the circulation. The membrane dynamics are also affected, as PI3K-C2α$^{WT/D1268A}$ platelets hardly form filopodia after stimulation, despite a normal phosphorylation of myosin light chain. The less developed and structured demarcation membrane system observed in PI3K-C2α$^{WT/D1268A}$ megakaryocytes suggests the membrane defects come from megakaryocytes and are not intrinsic to platelets.

Depending on the cell context, PI3K-C2α has been shown to produce PI3P and PI(3,4)P_2,[3,7,8,31] but whether this enzyme controls a housekeeping pool of these lipids or a pool generated after acute signaling is unknown. We show that in platelets, PI3K-C2α controls a basal PI3P pool that has a slow turnover but is not involved in the agonist-induced pool of PI3P. We did not find an implication of PI3K-C2α in the increased production of other phosphoinositides, including D3-phosphoinositides, after platelet activation. For instance, when PI3K-C2α is half inactivated, the production of PI(3,4)P_2

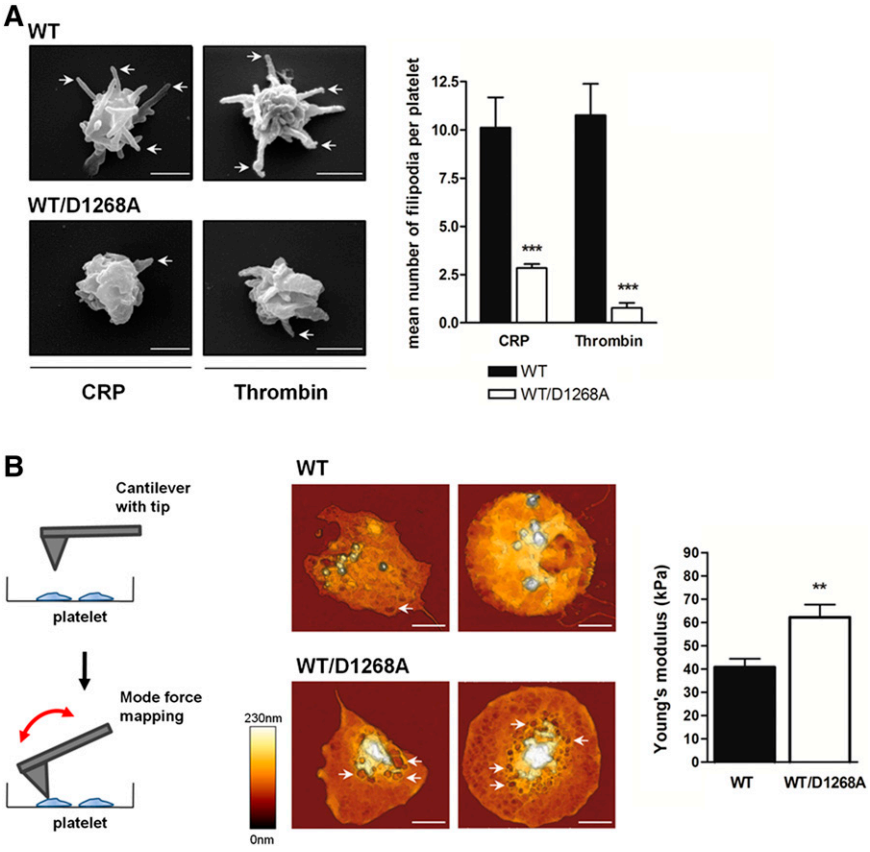

Figure 4. PI3K-C2α controls membrane dynamics and mechanical forces. (A) Washed platelets stimulated in suspension with CRP (10 μg/mL) and thrombin (0.5 IU/mL) were visualized by scanning electron microscopy. Images of 2 WT and PI3K-C2α$^{WT/D1268A}$ platelets are representative of 5 mice. Scale bar: 1 μm. Arrows show filopodia. Filopodia mean number was quantified per platelet (mean ± SEM; n = 3; $*P < .05$ and $**P < .01$ vs WT according to 2-tailed Student *t* test). (B) Schematic representation of AFM technique "force mapping mode," using a cantilever with tip to record platelet topography and measure the Young's modulus, inverse reflection of platelet elasticity. Washed platelets were placed on a fibrinogen-coated surface for 45 minutes in the presence of thrombin (0.5 IU/mL). Representative AFM images are shown and arrows indicate membrane invaginations. Scale bar: 1 μm. Quantitative determination of the local mechanical properties of live platelets was carried out by atomic force microscopy (JPK NWII), operating in force distance mode in liquid buffer solution at 37°C. The bar graph represents the platelet mean Young's modulus (mean ± SEM; n = 3; $**P < .01$, according to 2-tailed Student *t* test).

was not affected in platelets, which is in agreement with previous reports showing that a large part of PI(3,4)P_2 in platelets comes from the dephosphorylation of PI(3,4,5)P_3 by the 5-phosphatase SHIP1.[23] Thus, our results show that PI3K-C2α regulates a housekeeping pool of PI3P in platelets.

How can a defect in a particular pool of PI3P explain the membrane defect observed in PI3K-C2α$^{WT/D1268A}$ platelets? Our data show no differences in the major lipid composition and in microtubule thickness in these platelets but, rather, a deficiency in the membrane skeleton. The composition of the spectrin-based-membrane skeleton appears affected as spectrin itself, myosin, and filamin, moesin, GPIbα, and GPIIb are less abundant in this compartment. Spectrin-based membrane skeleton controls plasma membrane organization, stability, and shape and provides mechanical forces for the increment of elasticity and rigidity, which are needed to withstand the turbulence of blood circulation. Discontinuities in the skeleton may favor local inhomogeneities, creating specialized plasma membrane microdomains that may affect curvature and shape variation.[32] The spectrin-based membrane skeleton is critical for platelet membrane properties and has a strong effect on membrane shape and regulates the lateral distribution of the membrane glycoproteins to which it is attached.[27] It has recently been shown that the cortical actin-myosin-spectrin system brings external compressive forces during barbell-shaped proplatelet formation and determines platelet size.[15,19,33] This is important in the context of nonmuscle myosin MYH9-related diseases affecting platelets,[33] and possibly Bernard-Soulier syndrome, and may explain the large size and decreased number of platelets of these patients. Interestingly, membrane skeleton proteins such as β-spectrin and filamin, as well as myosin IIA and moesin, were identified in a screen of proteins able to interact with PI3P.[34,35] Conversely, vinculin that localizes to the membrane skeleton is normal in PI3K-C2α$^{WT/D1268A}$ platelets and was found not to bind PI3P.[36] Thus, loss of a PI3K-C2α-derived pool of PI3P with low turnover may induce a mislocalization/stabilization of proteins at the membrane skeleton, leading to modifications in membrane biophysical properties. PI3K-C2α has been shown to regulate clathrin-dependent endocytosis[3] and to play an important role in cargo delivery to the primary cilium.[7] In endothelial cells, deletion of PI3K-C2α leads to defective delivery of VE-cadherin to cell junctions, leading to impaired assembly of endothelial junctions.[8] The class II PI3K homolog in flies regulates endosomal sorting from the endocytic compartment to the plasma membrane.[37,38] Thus, PI3K-C2α is a central spatiotemporal player of membrane dynamics by acting at several levels, including membrane skeleton organization, clathrin-dependent endocytosis, and endocytic recycling.

In megakaryocytes and platelets, which require intense membrane plasticity and remodeling, partial inactivation of the kinase activity of PI3K-C2α has profound consequences. In addition to a disorganization of the membrane skeleton, defects in vesicular trafficking may also take place as suggested by α-granule defects. Although these structural defects have a minor effect on primary hemostasis, they are associated with a marked alteration in the function of platelets in arterial thrombosis. Interestingly, a very recent study by Mountford et al,[39] using knock-down mice models of PI3K-C2α, also highlights the key role of PI3K-C2α in the regulation of membrane structure and dynamics in platelets. In addition to similarities in the phenotypes of our KI and their knock-down models, several differences exist, including α-granule defects and thrombus stability, that may come from the putative scaffolding role of PI3K-C2α. In addition, by using a sensitive method to measure PI3P pools, we

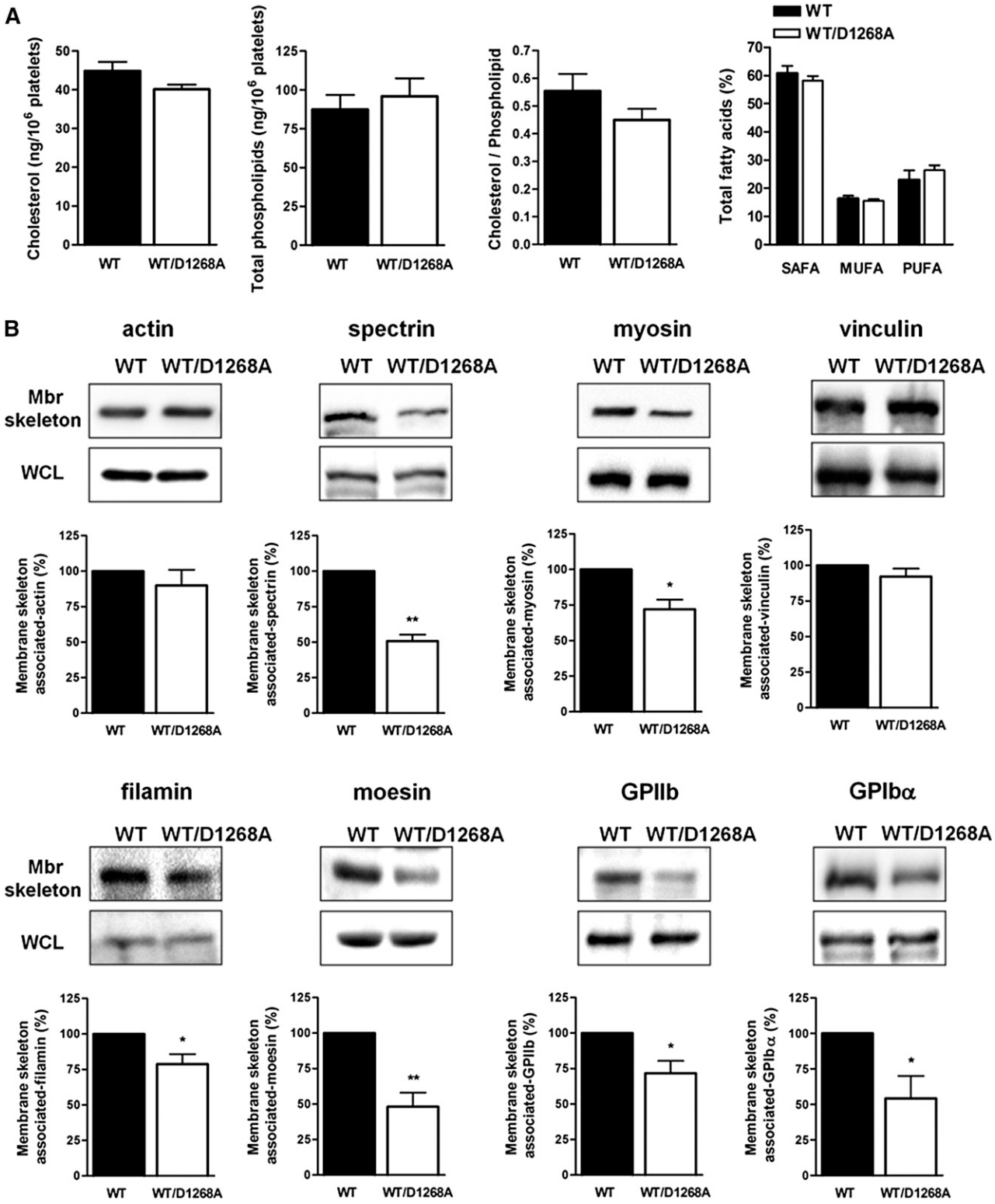

Figure 5. PI3K-C2α is a key regulator of plasma membrane/skeleton integrity. (A) Cholesterol, phospholipids, and fatty acids from resting platelets were analyzed as described in *Methods*. MUFA, monounsaturated fatty acids; PUFA, polyunsaturated fatty acids; SAFA, saturated fatty acids. (B) Western blot analysis of actin, spectrin, myosin, vinculin, filamin, moesin, GPIIb, and GPIbα from isolated membrane skeleton (Mbr skeleton) and whole lysates (WCL) of resting platelets (mean ± SEM; n = 4–7; $^{*}P < .05$, $^{**}P < .01$ vs WT according 1 sample *t* test).

provide evidence that defects in platelet biogenesis are linked to PI3K-C2α regulation of a PI3P housekeeping pool that was not observed by Mountford et al.

In conclusion, our study points to a new function of PI3K-C2α as a critical regulator of normal platelet ultrastructure through the control of membrane morphology and association with the cortical

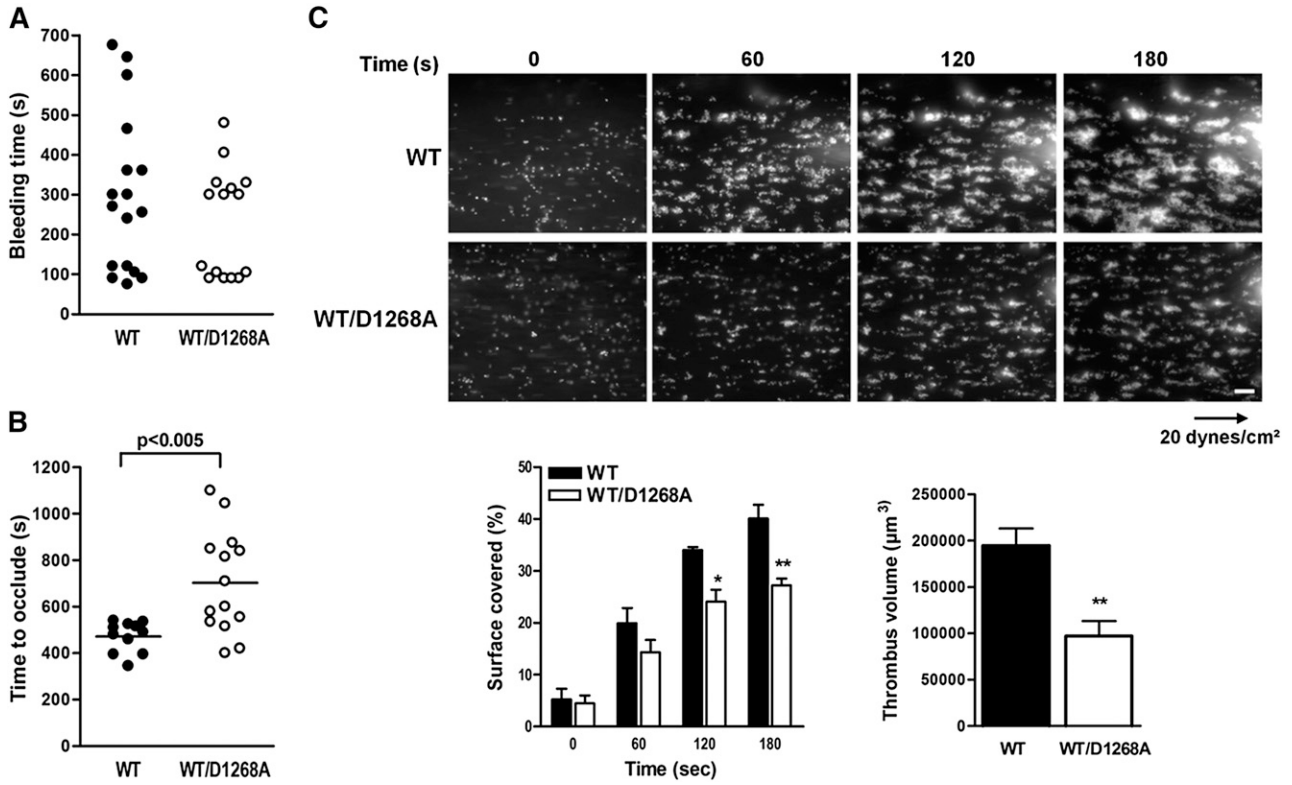

Figure 6. PI3K-C2α$^{WT/D1268A}$ mice exhibit defective platelet activation and prothrombotic capacity. (A) Tail bleeding time of WT (n = 17) and PI3K-C2α$^{WT/D1268A}$ (n = 18) mice was measured as described in *Methods*. (B) Thrombotic response of mice to ferric chloride injury of the carotid artery. Time to occlude (blood flow arrest) was measured in the carotid artery after exposure to 7.5% $FeCl_3$ for 3 minutes (mean ± SEM; n = 14 mice; $P < .005$ according to 2-tailed Student *t* test). (C) $DiOC_6$-labeled platelets in whole blood were perfused through a collagen-coated microcapillary at a shear rate of 20 dynes/cm^2 during 3 minutes. Thrombus formation was visualized in real time. Scale bar: 20 μm. Area covered by platelet thrombi and thrombus volume were measured using Image J software (mean ± SEM; n = 3; *$P < .05$, **$P < .01$ vs WT according to 2-tailed Student *t* test and 2-way ANOVA).

skeleton, with consequences on the level of circulating barbell-shaped proplatelets and on the arterial thrombosis function of platelets.

Acknowledgments

We thank the personnel of Anexplo animal facilities (US006/Centre Régional d'Exploration Fonctionnelle et de Ressources Expérimentales Inserm / Université Toulouse III) for animal handling and the Non-Invasive Exploration Service (US006/Centre Régional d'Exploration Fonctionnelle et de Ressources Expérimentales Inserm / Université Toulouse III) for the use of their irradiator, Genotoul Imaging facilities (INSERM U1048, R. D'angelo and M. Zanoun; Centre de Microscopie Electronique Appliqué à la Biologie/Université Toulouse III, B. Payre and I. Fourqaux), the cytometry facility of Inserm U1048 (A. Zakaroff-Girard and C. Pecher), the genomic and transcriptomic platform of Inserm U1048 (J. J. Maoret and F. Martins), and the lipidomic facility of Inserm U1048 (J. Bertrand-Michel). We thank J. Viaud for providing the FYVE^{HRS} probe and P. Valet for *Pik3c2a* gene RT-PCR primers. We also thank all members of the B.P. laboratory.

C.V. was supported by a PhD grant from Université Toulouse III. C.C. was supported by an EU Marie Curie fellowship (PIIF-GA-2009-252846). Work in the laboratory of B.P. was supported by Inserm (U104815B and SPDOTSEVERI) and the Fondation pour la Recherche Médicale (R13059BB). Work in the laboratory of B.V. was supported by the Medical Research Council (G0700755), the UK Biotechnology and Biological Sciences Research Council (BB/I007806/1), Cancer Research UK (C23338/A15965), the Ludwig Institute for Cancer Research, and the National Institute for Health Research University College London Hospitals Biomedical Research Centre. B.P. is a scholar of the Institut Universitaire de France.

Authorship

Contribution: C.V. and S.S. designed and performed most experiments and analyzed the data; C.C., M.A.W., and B.V. generated and carried out the basic characterization of the PI3K-C2α^{D1268A} mice; G.C. and B.P. designed and performed phosphoinositide analysis; C.S. performed AFM experiments; C.C. performed arterial thrombosis in vivo; F.G.-I. and M.-P.G. analyzed data; and B.P., B.V., and S.S. analyzed data and wrote the article.

Conflict-of-interest disclosure: B.V. is a consultant to Retroscreen (London, United Kingdom) and Karus Therapeutics (Oxford, United Kingdom).

Correspondence: Sonia Severin, INSERM, U1048-Université Toulouse III, Institut des Maladies Métaboliques et Cardiovasculaires, 1 Avenue Jean Poulhes, BP 84225, 31432 Toulouse Cedex 04, France; e-mail: sonia.severin@inserm.fr.

References

1. Di Paolo G, De Camilli P. Phosphoinositides in cell regulation and membrane dynamics. *Nature.* 2006;443(7112):651-657.
2. Vanhaesebroeck B, Guillermet-Guibert J, Graupera M, Bilanges B. The emerging mechanisms of isoform-specific PI3K signalling. *Nat Rev Mol Cell Biol.* 2010;11(5):329-341.
3. Posor Y, Eichhorn-Gruenig M, Puchkov D, et al. Spatiotemporal control of endocytosis by phosphatidylinositol-3,4-bisphosphate. *Nature.* 2013;499(7457):233-237.
4. Devereaux K, Dall'Armi C, Alcazar-Roman A, et al. Regulation of mammalian autophagy by class II and III PI 3-kinases through PI3P synthesis. *PLoS One.* 2013;8(10):e76405.
5. Falasca M, Maffucci T. Regulation and cellular functions of class II phosphoinositide 3-kinases. *Biochem J.* 2012;443(3):587-601.
6. Fan CW, Chen B, Franco I, et al. The Hedgehog pathway effector smoothened exhibits signaling competency in the absence of ciliary accumulation. *Chem Biol.* 2014;21(12): 1680-1689.
7. Franco I, Gulluni F, Campa CC, et al. PI3K class II α controls spatially restricted endosomal PtdIns3P and Rab11 activation to promote primary cilium function. *Dev Cell.* 2014;28(6):647-658.
8. Yoshioka K, Yoshida K, Cui H, et al. Endothelial PI3K-C2α, a class II PI3K, has an essential role in angiogenesis and vascular barrier function. *Nat Med.* 2012;18(10):1560-1569.
9. Zhang J, Banfić H, Straforini F, Tosi L, Volinia S, Rittenhouse SE. A type II phosphoinositide 3-kinase is stimulated via activated integrin in platelets. A source of phosphatidylinositol 3-phosphate. *J Biol Chem.* 1998;273(23): 14081-14084.
10. George JN. Platelets. *Lancet.* 2000;355(9214): 1531-1539.
11. Hartwig JH. The platelet: form and function. *Semin Hematol.* 2006;43(1 Suppl 1):S94-S100.
12. Chang Y, Bluteau D, Debili N, Vainchenker W. From hematopoietic stem cells to platelets. *J Thromb Haemost.* 2007;5(Suppl 1):318-327.
13. Behnke O, Forer A. From megakaryocytes to platelets: platelet morphogenesis takes place in the bloodstream. *Eur J Haematol Suppl.* 1998; 61:3-23.
14. Junt T, Schulze H, Chen Z, et al. Dynamic visualization of thrombopoiesis within bone marrow. *Science.* 2007;317(5845):1767-1770.
15. Patel-Hett S, Wang H, Begonja AJ, et al. The spectrin-based membrane skeleton stabilizes mouse megakaryocyte membrane systems and is essential for proplatelet and platelet formation. *Blood.* 2011;118(6):1641-1652.
16. Poirault-Chassac S, Nguyen KA, Pietrzyk A, et al. Terminal platelet production is regulated by von Willebrand factor. *PLoS One.* 2013;8(5):e63810.
17. Schwertz H, Köster S, Kahr WH, et al. Anucleate platelets genere progeny. *Blood.* 2010;115(18): 3801-3809.
18. Thon JN, Italiano JE Jr. Does size matter in platelet production? *Blood.* 2012;120(8): 1552-1561.
19. Thon JN, Macleod H, Begonja AJ, et al. Microtubule and cortical forces determine platelet size during vascular platelet production. *Nat Commun.* 2012;3:852.
20. Thon JN, Montalvo A, Patel-Hett S, et al. Cytoskeletal mechanics of proplatelet maturation and platelet release. *J Cell Biol.* 2010;191(4): 861-874.
21. Severin S, Gaits-Iacovoni F, Allart S, Gratacap MP, Payrastre B. A confocal-based morphometric analysis shows a functional crosstalk between the actin filament system and microtubules in thrombin-stimulated platelets. *J Thromb Haemost.* 2013;11(1):183-186.
22. Chicanne G, Severin S, Boscheron C, et al. A novel mass assay to quantify the bioactive lipid PtdIns3P in various biological samples. *Biochem J.* 2012;447(1):17-23.
23. Giuriato S, Pesesse X, Bodin S, et al. SH2-containing inositol 5-phosphatases 1 and 2 in blood platelets: their interactions and roles in the control of phosphatidylinositol 3,4,5-trisphosphate levels. *Biochem J.* 2003;376(Pt 1):199-207.
24. Hutter JL, Bechhoefer J. Calibration of atomic-force microscope tips. *Rev Sci Instrum.* 1993; 64(7):1868-1873.
25. Sneddon IN. The relation between load and penetration in the axisymmetric problem for a punch of arbitrary profile. *Int J Eng Sci.* 1965; 3(1):47-57.
26. Payrastre B. Phosphoinositides: lipid kinases and phosphatases. *Methods Mol Biol.* 2004;273: 201-212.
27. Fox JE, Boyles JK. The membrane skeleton–a distinct structure that regulates the function of cells. *BioEssays.* 1988;8(1):14-18.
28. Italiano JE Jr. Unraveling mechanisms that control platelet production. *Semin Thromb Hemost.* 2013; 39(1):15-24.
29. Hartwig J, Italiano J Jr. The birth of the platelet. *J Thromb Haemost.* 2003;1(7):1580-1586.
30. Thon JN, Italiano JE. Platelets: production, morphology and ultrastructure. *Handb Exp Pharmacol.*2012(210):3-22.
31. Mazza S, Maffucci T. Class II phosphoinositide 3-kinase C2alpha: what we learned so far. *Int J Biochem Mol Biol.* 2011;2(2):168-182.
32. De Matteis MA, Morrow JS. Spectrin tethers and mesh in the biosynthetic pathway. *J Cell Sci.* 2000;113(Pt 13):2331-2343.
33. Spinler KR, Shin JW, Lambert MP, Discher DE. Myosin-II repression favors pre/proplatelets but shear activation generates platelets and fails in macrothrombocytopenia. *Blood.* 2015;125(3): 525-533.
34. Catimel B, Kapp E, Yin MX, et al. The PI(3)P interactome from a colon cancer cell. *J Proteomics.* 2013;82:35-51.
35. Gunn-Moore FJ, Welh GI, Herron LR, et al. A novel 4.1 ezrin radixin moesin (FERM)-containing protein, 'Willin'. *FEBS Lett.* 2005;579(22): 5089-5094.
36. Steimle PA, Hoffert JD, Adey NB, Craig SW. Polyphosphoinositides inhibit the interaction of vinculin with actin filaments. *J Biol Chem.* 1999; 274(26):18414-18420.
37. Jean S, Cox S, Schmidt EJ, Robinson FL, Kiger A. Sbf/MTMR13 coordinates PI(3)P and Rab21 regulation in endocytic control of cellular remodeling. *Mol Biol Cell.* 2012; 23(14):2723-2740.
38. Velichkova M, Juan J, Kadandale P, et al. Drosophila Mtm and class II PI3K coregulate a PI(3)P pool with cortical and endolysosomal functions. *J Cell Biol.* 2010;190(3):407-425.
39. Mountford JK, Petitjean C, Putra HW, et al. The class II PI 3-kinase, PI3KC2α, links platelet internal membrane structure to shear-dependent adhesive function. *Nat Commun.* 2015;6:6535.